#### **OPEN ACCESS**



# Scattering of Superthermal Ions at Shocks: Dependence on Energy

Michael Gedalin , Natalia Ganushkina , Nikolai V. Pogorelov , on and Vadim Roytershteyn Department of Physics, Ben Gurion University of the Negev, Beer-Sheva, Israel; gedalin@bgu.ac.il Finnish Meteorological Institute, Helsinki, Finland Climate and Space Science and Engineering Department, University of Michigan, Ann Arbor, MI, USA Department of Space Science, The University of Alabama in Huntsville, AL 35805, USA Center for Space Plasma and Aeronomic Research, The University of Alabama in Huntsville, AL 35805, USA Space Science Institute, Boulder, CO 80301, USA Received 2023 October 11; revised 2023 October 17; accepted 2023 October 17; published 2023 November 6

#### **Abstract**

Diffusive shock acceleration requires the production of backstreaming superthermal ions (injection) as a first step. Such ions can be generated in the process of scattering of ions in the superthermal tail off the shock front. Knowledge of the scattering of high-energy ions is essential for matching conditions of upstream and downstream distributions at the shock transition. Here we analyze the generation of backstreaming ions as a function of their initial energy in a model stationary shock and in a similar rippled shock. Rippling substantially enhances ion reflection and the generation of backstreaming ions for slightly and moderately superthermal energies, and thus is capable of ensuring ion injection into a further diffusive shock acceleration process. For high-energy ions, there is almost no difference in the fraction of backstreaming ions produced and the ion distributions between the planar stationary shock and the rippled shock.

Unified Astronomy Thesaurus concepts: Shocks (2086); Planetary bow shocks (1246); Interplanetary shocks (829)

#### 1. Introduction

Collisionless shocks are ubiquitous in space plasmas. In these shocks, the energy of the incident flow is used for plasma heating, particle acceleration, and magnetic field enhancement -via interaction between charged particles and electromagnetic fields collectively produced by these particles themselves (see Treumann 2009, for a review). Acceleration of a small fraction of charged particles to high energies occurs via diffusive shock acceleration (DSA; Drury 1983). DSA requires a seed population of superthermal particles, which propagate from the shock into the upstream region (the socalled injection; Malkov & Völk 1998; Scholer et al. 1998). Backstreaming (or escaping) ions are produced in shocks via ion reflection (Hudson 1965). Such ions are observed as fieldaligned beams near the Earth's bow shock (Thomsen et al. 1983; Kucharek et al. 2004; Meziane et al. 2004) and as energetic reflected ions at interplanetary shocks (Zhou et al. 2020). The mechanism of generation of these ions is not completely understood. They were shown to be naturally produced by reflection in oblique shocks with the angle between the shock normal and the upstream magnetic field vector  $\theta_{Bn}$  < 50° (Leroy & Winske 1983; Tanaka et al. 1983; Burgess 1987; Gedalin et al. 2008), but they are also observed at shocks with larger  $\theta_{Bn}$  (Kucharek et al. 2004). With increasing upstream Mach number collisionless shocks become rippled (Moullard et al. 2006; Lobzin et al. 2008; Johlander et al. 2016, 2018; Gingell et al. 2017). It was shown (Gedalin et al. 2023) that some ions reflected by a rippled shock may escape into the upstream region. These ions come to the shock in the tail of the distribution. It was shown also that superthermal tails result in the enhancement of ion

Original content from this work may be used under the terms of the Creative Commons Attribution 4.0 licence. Any further distribution of this work must maintain attribution to the author(s) and the title of the work, journal citation and DOI.

reflection (Gedalin & Ganushkina 2022a). Thus, rippling and the presence of superthermal incident ions may be important for injection. Pickup ions, which are completely superthermal, are efficiently reflected and escape (Gedalin et al. 2021). Let  $V_u$ be the incident plasma flow velocity along the shock normal in the shock frame and  $m_p$  the ion (proton) mass. Most pickup ions have energies  $\approx m_p V_u^2/2$ . The dependence of reflection on the ion energy  $\epsilon$  in the range  $0 < \epsilon < m_p V_u^2/2$  has not been analyzed so far. Knowledge of the dependence on energies well above  $m_p V_u^2/2$  is important for imposing proper matching conditions at the shock for the DSA-accelerated ions (Drury 1983; Gieseler et al. 1999; Kirk & Dendy 2001). So far only the scattering probabilities of high-energy ions have been analyzed (Gedalin et al. 2016). Here we study the dependence of ion reflection on the incident energy using analysis of test particles in a planar stationary shock and in its rippled counterpart.

## 2. Notation

We denote by u and d the upstream and downstream regions, respectively. Ions enter the shock from the upstream and either proceed to the downstream region (transmitted and reflected-transmitted ions) or are reflected and escape upstream (backstreaming ions). In a planar stationary shock, all fields depend only on the spatial coordinate along the shock normal, which is chosen as the x-direction here. The upstream magnetic field is  $\mathbf{B}_u = B_u(\cos\theta_{Bn}, 0, \sin\theta_{Bn})$ . The normal incidence frame (NIF) is the frame in which the shock is not moving and the upstream plasma flows along the shock normal with speed  $V_u$ . The de Hoffman–Teller frame (HT) is the shock frame in which the upstream flow velocity is along the upstream magnetic field,  $V_u^{(\text{HT})} = V_u(1, 0, \tan\theta_{Bn})$ . We limit ourselves to non-relativistic speeds  $V_u \ll c$ ,  $V_u \tan\theta_{Bn} \ll c$ , where c is the speed

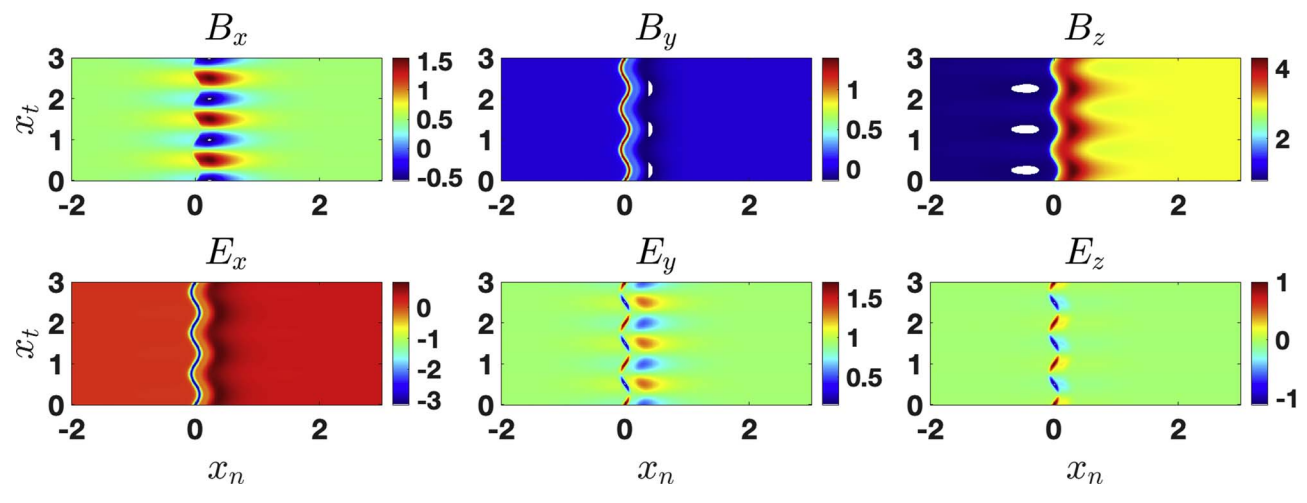


Figure 1. Magnetic and electric fields for the rippled shock with the parameters in the text. Here  $x_n$  is the coordinate along the shock normal, and  $x_t$  is the coordinate along the shock front in the direction of rippled propagation.

of light. Then  $\mathbf{B}^{(HT)} = \mathbf{B}^{(NIF)}$  and

$$E_y^{(HT)} = E_y^{(NIF)} - \frac{V_u B_x^{(NIF)} \tan \theta_{Bn}}{C}$$
 (1)

$$E_x^{(\text{HT})} = E_x^{(\text{NIF})} + \frac{V_u B_y^{(\text{NIF})} \tan \theta_{Bn}}{c}.$$
 (2)

For simplicity, we consider a plasma consisting of electrons and protons, with equal upstream number densities  $n_u$ . The upstream ion gyrofrequency is  $\Omega_u = eB_u/m_pc$ , and the upstream ion plasma frequency is  $\omega_{pi} = \sqrt{4\pi n_u e^2/m_p}$ . The ion inertial length is  $c/\omega_{pi}$ . The Alfvén speed is  $v_{\rm A}=c\Omega_u/\omega_{pi}$  and the Alfvénic Mach number is  $M = V_u/v_A$ . In what follows, only this Mach number is used. The upstream ion convective gyroradius is  $\rho_i = V_u/\Omega_u = M(c/\omega_{pi})$ . In what follows we use the normalized variables

$$x/\rho_i \to x$$
,  $v/V_u \to v$ ,  $\Omega_u t \to t$  (3)

and the electric field is normalized to  $V_{\mu}B_{\mu}/c$ . The cross-shock potentials in both NIF and HT are normalized as follows:

$$s = e\phi/(m_p V_u^2/2) = \left(-e \int E_x dx\right)/(m_p V_u^2/2).$$
 (4)

#### 3. Shock Model

The chosen shock model is described in detail in Gedalin et al. (2023). The normalized stationary planar fields are given

$$B_x = \cos \theta_{Bn}, \quad B_z = B \sin \theta_{Bn}, \quad B_y = k_B \left(\frac{dB}{dx}\right),$$
 (5)

$$E_x = -k_E \left(\frac{dB}{dx}\right), \quad E_y = \sin \theta_{Bn}, \quad E_z = 0,$$
 (6)

$$B = B_1 + B_2, \tag{7}$$

$$B_1 = \frac{R_1 - 1}{2} + \frac{R_1 + 1}{2} \tanh \frac{3x}{D},\tag{8}$$

$$B_2 = R_2 \left( 1 - \tanh \frac{3(x - X_r)}{W_r} \right) \left( 1 + \tanh \frac{3(x - X_l)}{W_l} \right). \tag{9}$$

In these expressions  $B_1$  describes the basic profile. The downstream magnetic field is

$$B_d = \sqrt{R_1^2 \sin^2 \theta_{Bn} + \cos^2 \theta_{Bn}}.$$
 (10)

The part  $B_2$  describes an overshoot. The coefficients  $k_E$  and  $k_B$  are obtained from the normalized cross-shock potentials  $s^{(NIF)}$ and  $s^{(\mathrm{HT})}$ . The parameters  $\theta_{Bn},\,B_d,\,R_2,\,s_{\mathrm{NIF}},\,s_{\mathrm{HT}},\,D,\,X_l,\,X_r,\,W_l,$ and  $W_r$  completely define the chosen model of a planar stationary shock profile.

In order to add rippling, we replace (Gedalin & Ganushkina 2022b; Gedalin et al. 2023)

$$x \to X = x - a\psi g \tag{11}$$

$$\psi(y, z, t) = \sin(k_r(z\cos\varphi + y\sin\varphi - V_r t)) \tag{12}$$

$$g(x) = \left(1 + \tanh \frac{3(x - X_L)}{W_L}\right) \left(1 - \tanh \frac{3(x - X_R)}{W_R}\right)$$
 (13)

$$B(x) \to B(X)$$
 (14)

so that in NIF

$$B_x = k_B \left(\frac{dB}{dX}\right) \left(\frac{\partial X}{\partial y}\right) - B\sin\theta_{Bn} \left(\frac{\partial X}{\partial z}\right) + \cos\theta_{Bn}$$
 (15)

$$B_{y} = -k_{B} \left(\frac{dB}{dX}\right) \left(\frac{\partial X}{\partial x}\right) \tag{16}$$

$$B_z = B \sin \theta_{Bn} \left( \frac{\partial X}{\partial x} \right) \tag{17}$$

$$E_x = -k_E \left(\frac{dB}{dX}\right) \left(\frac{\partial X}{\partial x}\right) \tag{18}$$

$$E_{y} = \sin \theta_{Bn} - B \sin \theta_{Bn} \left( \frac{\partial X}{\partial t} \right) - k_{E} \left( \frac{dB}{dX} \right) \left( \frac{\partial X}{\partial y} \right)$$
 (19)

$$E_z = -k_B \left(\frac{dB}{dX}\right) \left(\frac{\partial X}{\partial t}\right) - k_E \left(\frac{dB}{dX}\right) \left(\frac{\partial X}{\partial z}\right). \tag{20}$$

The ripples in the model are moving along the shock front with velocity  $V_r = V_r(0, \sin \varphi, \cos \varphi)$ . In the frame of the ripples, the fields become time-independent. The speed is  $V_r \ll c$ (Johlander et al. 2016, 2018; Gingell et al. 2017; Omidi et al. 2021), so the transformation of the fields from NIF to this

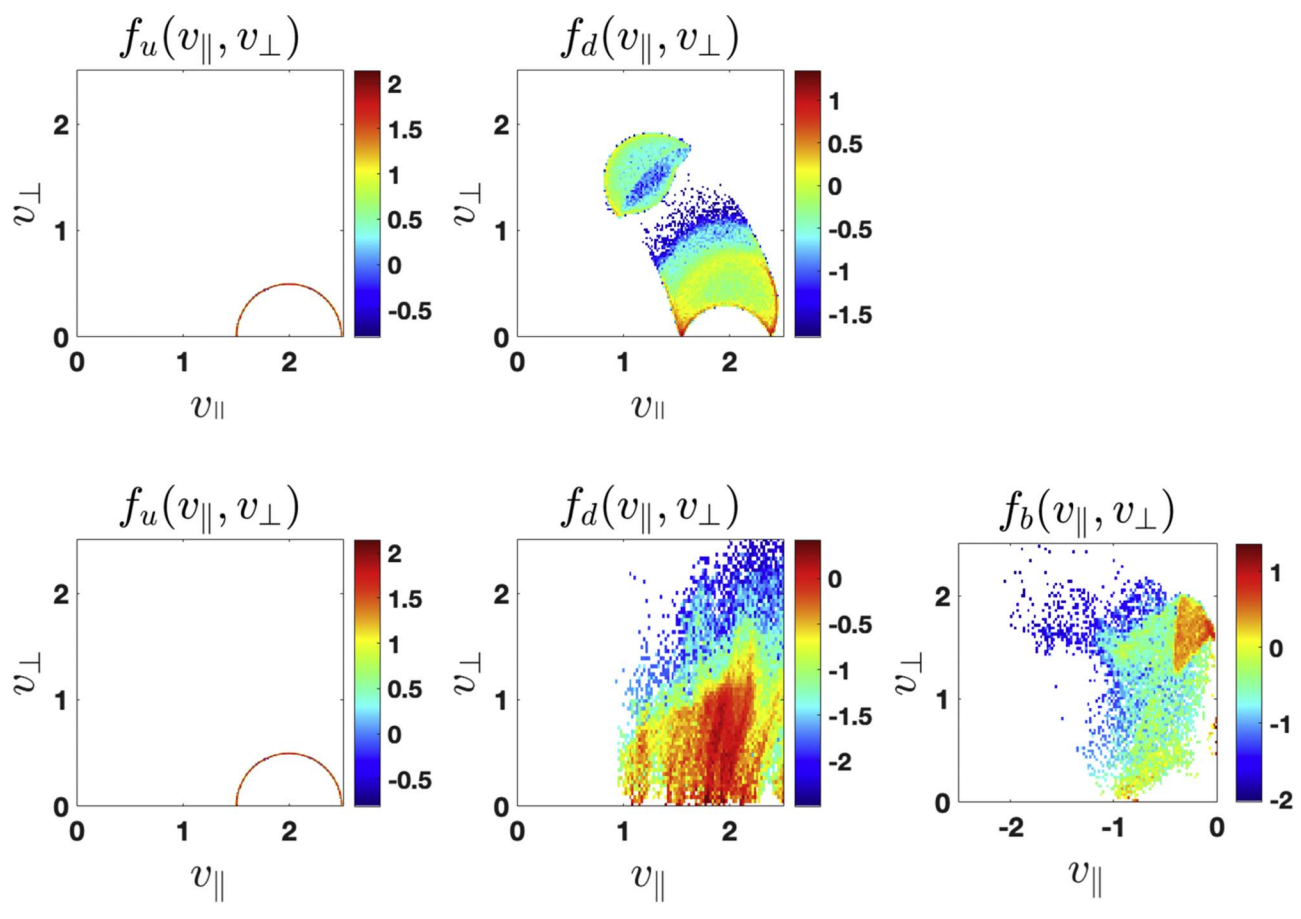


Figure 2. Left column: the distribution of the forward-moving incident ions  $f_u(\nu_{\parallel}, \nu_{\perp})$  (see explanation in text). Upper middle: the distribution of the ions far downstream of the shock  $f_d(\nu_{\parallel}, \nu_{\perp})$  without rippling. Bottom middle: the distribution of the ions far downstream of the shock  $f_d(\nu_{\parallel}, \nu_{\perp})$  in the rippled shock. Upper right (empty in this case): the distribution of the backstreaming ions  $f_b(\nu_{\parallel}, \nu_{\perp})$  without rippling. Bottom right: the distribution of the backstreaming ions  $f_b(\nu_{\parallel}, \nu_{\perp})$  in the rippled shock. The initial ion distribution is isotropic with  $\nu_p = 0.5$ .

frame yields

$$E_x' = E_x + V_r \sin \varphi B_z - V_r \cos \varphi B_y \tag{21}$$

$$E_{v}' = E_{v} + V_{r} \cos \varphi B_{x} \tag{22}$$

$$E_z' = E_z - V_r \sin \varphi B_r. \tag{23}$$

#### 4. Test Particle Analysis

We numerically solve the equations of motion

$$\frac{d\mathbf{r}}{dt} = \mathbf{v}, \quad \frac{d\mathbf{v}}{dt} = \mathbf{E} + \mathbf{v} \times \mathbf{B} \tag{24}$$

in the model fields above. In the case of a stationary planar shock, the computation is done in NIF. In the case of a rippled shock, we switch to the frame of the ripples. Solving the equations of motion is equivalent to solving the Vlasov equation for the distribution function f(t, r, v), which is constant along the trajectory, given by a solution of Equation (24). For each particle with the initial velocity  $v_0$ , we numerically find the final velocity  $v_f$  far from the shock, either downstream or upstream, depending on the behavior of the ion. The initial and final velocities are shifted into HT and the components parallel and perpendicular to the local magnetic field,  $v_{\parallel}$  and  $v_{\perp}$ , are determined. In the upstream and downstream regions of HT each ion freely streams along

the magnetic field and gyrates around the magnetic field, without any drift across the magnetic field, so that the distribution function depends only on  $v_{\parallel}$  and  $v_{\perp}$ . The conservation of a number of particles requires

$$\int v_{0,\parallel} f_0(v_{0,\parallel}, v_{0,\perp}) dv_{0,\parallel} v_{0,\perp} dv_{0,\perp} 
= \int v_{f,\parallel} f_f(v_{f,\parallel}, v_{f,\perp}) dv_{f,\parallel} v_{f,\perp} dv_{f,\perp}.$$
(25)

In order to find  $f_f(v_{f,\parallel}, v_{f,\perp})$  numerically, we create a grid in the  $v_{\parallel}-v_{\perp}$  space, and each particle with final velocity in the range  $[v_{\parallel}, v_{\parallel} + \Delta v_{\parallel}, v_{\perp}, v_{\perp} + \Delta v_{\perp}]$  is assigned the weight  $v_{0,\parallel}/v_{f,\parallel}$ . The incident particle distribution  $f_0(v_{0,\parallel}, v_{0,\perp})dv_{0,\parallel}v_{0,\perp}dv_{0,\perp}$  is generated numerically. Summing up all particles with their weights within each grid cell, we numerically derive the distribution function  $f_f(v_{f,\parallel}, v_{f,\perp})$ . In the planar stationary shock, the initial position is the same for all incident particles. For a rippled shock for proper spatial averaging along the shock front, the incident y and z positions are uniformly distributed within one ripple wavelength.

# 5. Ion Distributions

In the present test particle analysis, the following parameters have been used: M=6,  $B_d=3$ ,  $R_2=1$ ,  $X_l=X_r=0.5$ ,  $W_l=D$ ,  $W_r=2D$ ,  $\theta_{Bn}=60^\circ$ , D=2/M,  $s^{(\rm NIF)}=0.4$ , and  $s^{(\rm HT)}=0.1$ . The rippling parameters are:  $\varphi=45^\circ$ ,  $k_r=2\pi$ ,  $v_r=1$ ,

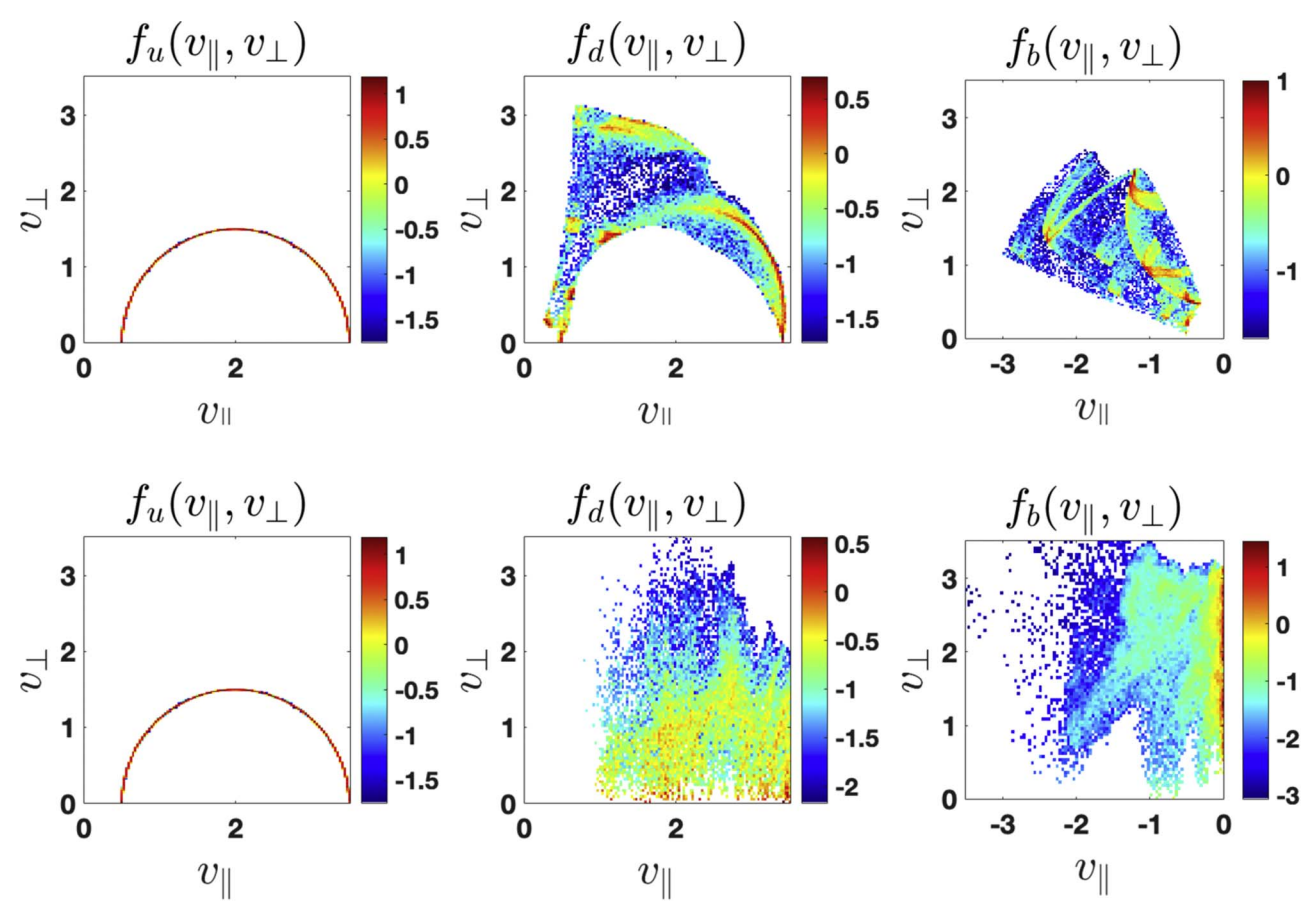


**Figure 3.** Left column: the distribution of the forward-moving incident ions  $f_u(v_{\parallel}, v_{\perp})$  (see explanation in text). Upper middle: the distribution of the ions far downstream of the shock  $f_d(v_{\parallel}, v_{\perp})$  without rippling. Bottom middle: the distribution of the ions far downstream of the shock  $f_d(v_{\parallel}, v_{\perp})$  in the rippled shock. Upper right: the distribution of the backstreaming ions  $f_b(v_{\parallel}, v_{\perp})$  without rippling. Bottom right: the distribution of the backstreaming ions  $f_b(v_{\parallel}, v_{\perp})$  in the rippled shock. The initial ion distribution is isotropic with  $v_p = 1.5$ .

 $X_L = X_R = 0$ , and  $W_L = W_R = 2$ . Figure 1 shows the electric and magnetic fields of the rippled shock. Rippling is interpreted as a wave in the foot (Gingell et al. 2017) or in the overshoot (Johlander et al. 2018). The proposed analytical model for rippling (Gedalin & Ganushkina 2022b) is not self-consistent but satisfies the Maxwell equations. As can be seen in Figure 1, both the upstream and downstream regions around the ramp (the region of the steepest magnetic field increase) are affected.

For the present analysis the incident distributions are isotropic shells of different velocities  $v_p$  and thickness of  $\Delta v_p = 0.01$  around the plasma velocity  $V_u$ , that is,  $v_p \leqslant |v - V_u| \leqslant v_p + \Delta v_p$ . Any isotropic incident distribution can be represented as a weighted superposition of such shells. We start with slightly superthermal ions,  $v_p = 0.5$ . It is widely accepted to describe a plasma with the upstream ion temperature  $T_u$  using the parameter  $\beta_i = 8\pi n_u T_u/B_u^2$ . The normalized thermal speed of ions is then  $v_T = \sqrt{\beta_i/2}/M$ . For the chosen Mach number,  $v_p = 3v_T$  if  $\beta_i = 2$ . Thus, for small  $\beta_i$  these ions are substantially superthermal for an upstream Maxwellian distribution, while for large  $\beta_i$  the chosen  $v_p = 0.5$  is in the tail of the Maxwellian and their number is not negligible.

All subsequent figures have the same format. The upper row is for the planar stationary shock and the bottom row is for the rippled shock, as specified in the above model. The left column shows the distribution of ions moving initially toward the

shock,  $\nu_{\parallel} > 0$ . Only these ions are included in the analysis. The top and bottom panels of this column are identical since this condition is imposed well upstream of the shock where the rippling effects are negligible. The middle column shows the distribution of ions that cross the shock, either not being reflected at all (directly transmitted ions) or after one or more reflections (reflected–transmitted ions). The right column shows the distribution of backstreaming ions, which eventually appear in the analysis well upstream of the shock with  $\nu_{\parallel} < 0$ . If there are no such ions, the corresponding panel is empty. The distributions are shown on a logarithmic scale.

Figure 2 shows the results of the test particle analysis for  $v_p = 0.5$ . In this case, all ions in the initial shell are moving toward the shock, as seen in the left column. In the upper middle panel, two populations are clearly seen: the lower  $v_{\perp}$ population of the directly transmitted ions, which were not reflected at all, and the higher  $v_{\perp}$  population of the reflectedtransmitted ions, which were reflected once and crossed the shock again. The upper right panel shows the ions that were reflected and escaped into the upstream region (backstreaming ions). In Figure 2 this panel is empty since no backstreaming ions were found for 80,000 ions entering the shock. The downstream distribution in the bottom middle panel (the rippled shock) is much more diffuse, which is not surprising since it includes ions crossing the shock at different positions with different local normals (Ofman & Gedalin 2013). Local normal is the direction of the steepest increase in |B| and

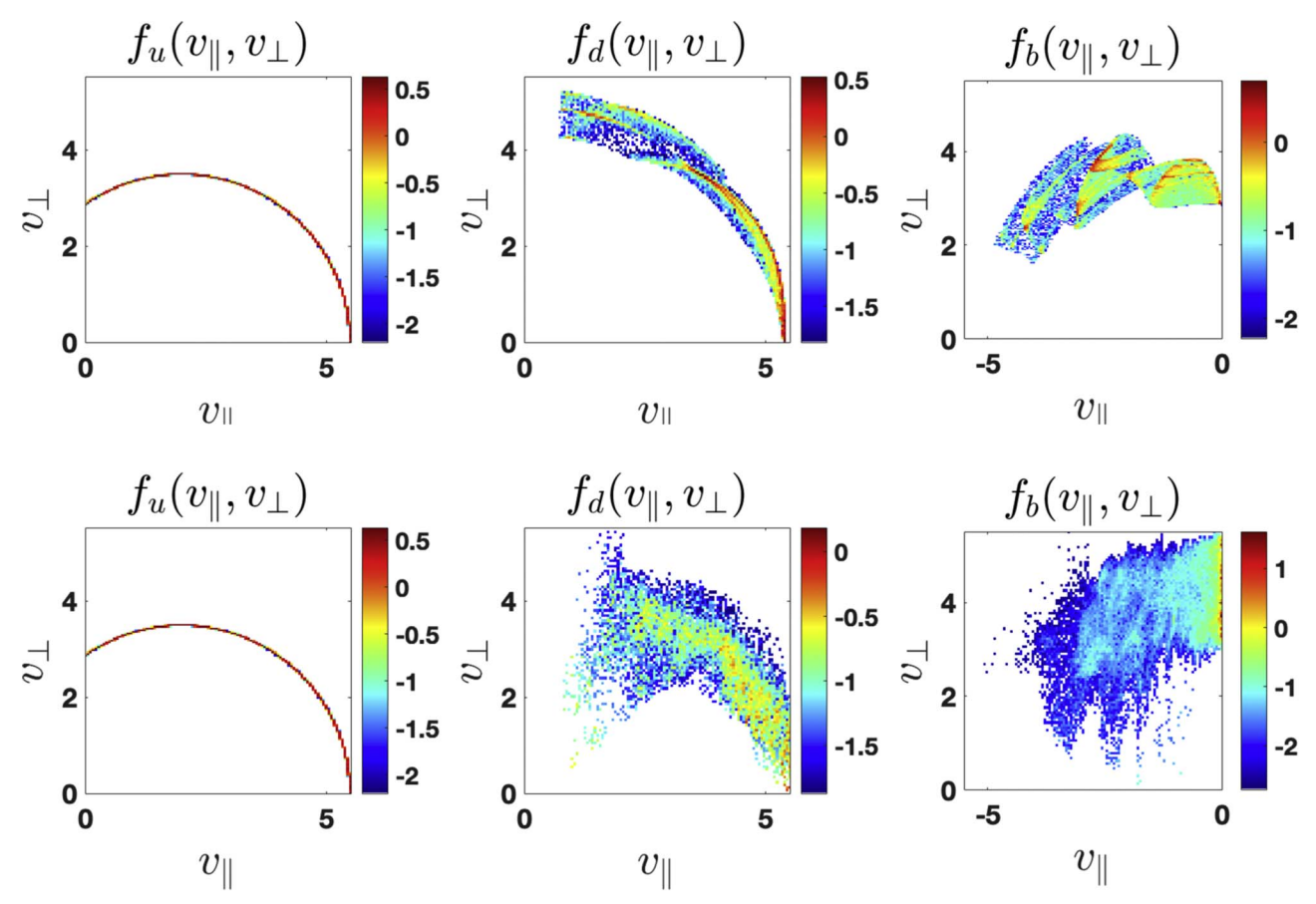


Figure 4. Left column: the distribution of the forward-moving incident ions  $f_u(v_{\parallel}, v_{\perp})$  (see explanation in text). Upper middle: the distribution of the ions far downstream of the shock  $f_d(v_{\parallel}, v_{\perp})$  without rippling. Bottom middle: the distribution of the ions far downstream of the shock  $f_d(v_{\parallel}, v_{\perp})$  in the rippled shock. Upper right: the distribution of the backstreaming ions  $f_b(v_{\parallel}, v_{\perp})$  without rippling. Bottom right: the distribution of the backstreaming ions  $f_b(v_{\parallel}, v_{\perp})$  in the rippled shock. The initial ion distribution is isotropic with  $v_p = 3.5$ .

depends on the position along the shock front in a rippled shock. About 20% of the incident ions are reflected and escape into the upstream region, making up the population of backstreaming ions, seen in the bottom right panel. This distribution is also very diffuse, with two maxima: one at low  $v_{\parallel}$  but large  $v_{\perp} \approx 1.5$  (a gyrating beam), and the other one at large  $v_{\parallel} \approx -1$  but low  $v_{\perp}$  (a field-aligned beam). As is mentioned above, the number of incident ions with  $v_p = 0.5$  for upstream Maxwellian ions is low unless  $\sqrt{\beta_i/2/M}$  is large enough. On average  $\beta_i \approx 1$  in the solar wind (Wilson et al. 2018). However, the distribution may be not Maxwellian but may have a long tail, like in a  $\kappa$ -distribution (see, e.g., Nicolaou et al. 2018, and references therein), so that the number of ions with  $v_p = 0.5$  may be small but non-negligible. Therefore, rippling of high-Mach-number shocks may appear to provide a mechanism for producing backstreaming ions from initially thermal distributions, thus solving the problem of injection.

Once escaping into the upstream region, the backstreaming ions may be scattered by fluctuations in the plasma with the magnetic field and eventually come back to the shock front. At this second entry to the shock these ions are already substantially superthermal. How the diffusive acceleration proceeds depends significantly on the behavior of these ions at the shock front.

Pickup ions with  $v_p = 1$  are known to be efficiently reflected and relatively easily escape into the upstream region even without rippling (Gedalin et al. 2021). Here we are interested in higher energies of incident ions. Figure 3 compares the ion

distributions at the shocks without and with the rippling, for  $v_p = 1.5$ . In this case, all ions are moving toward the shock initially. Without rippling 40% of the ions escape into the upstream region. Rippling increases this fraction to 47%. The downstream distribution in the rippled shock is much more diffuse but the maximum roughly follows the maximum for the planar stationary shock. The backstreaming ion distribution fills a much larger velocity space in the case of the rippled shock.

Figure 4 compares the ion distributions at the shocks without and with the rippling, for higher speeds,  $v_p = 3.5$ . In this case, only 63,000 ions of the 80,000 ions in the shell are moving toward the shock. Of these ions 74% and 79% escape without and with rippling, respectively. The distributions in the rippled shock are still more diffuse but already closely follow the distributions in the planar stationary shock, which is consistent with the understanding that only the change in global magnetic field from upstream to downstream is important for the dynamics of high-energy particles, while the details of the shock structure become progressively less important with the increase in energy. This is further emphasized by Figure 5, which shows the distributions for  $v_p = 10.5$ . The fractions of the backstreaming ions almost do not change compared to the case  $v_p = 3.5$ . Further increase of the speed shows that about 75% of the incident forward moving ions are reflected to form the backstreaming population.

For the same shock parameters and with the only change  $\theta_{Bn} = 80^{\circ}$  no substantial changes were found for  $v_p \ge 10.5$ ; about 70% of the incident ions escape.

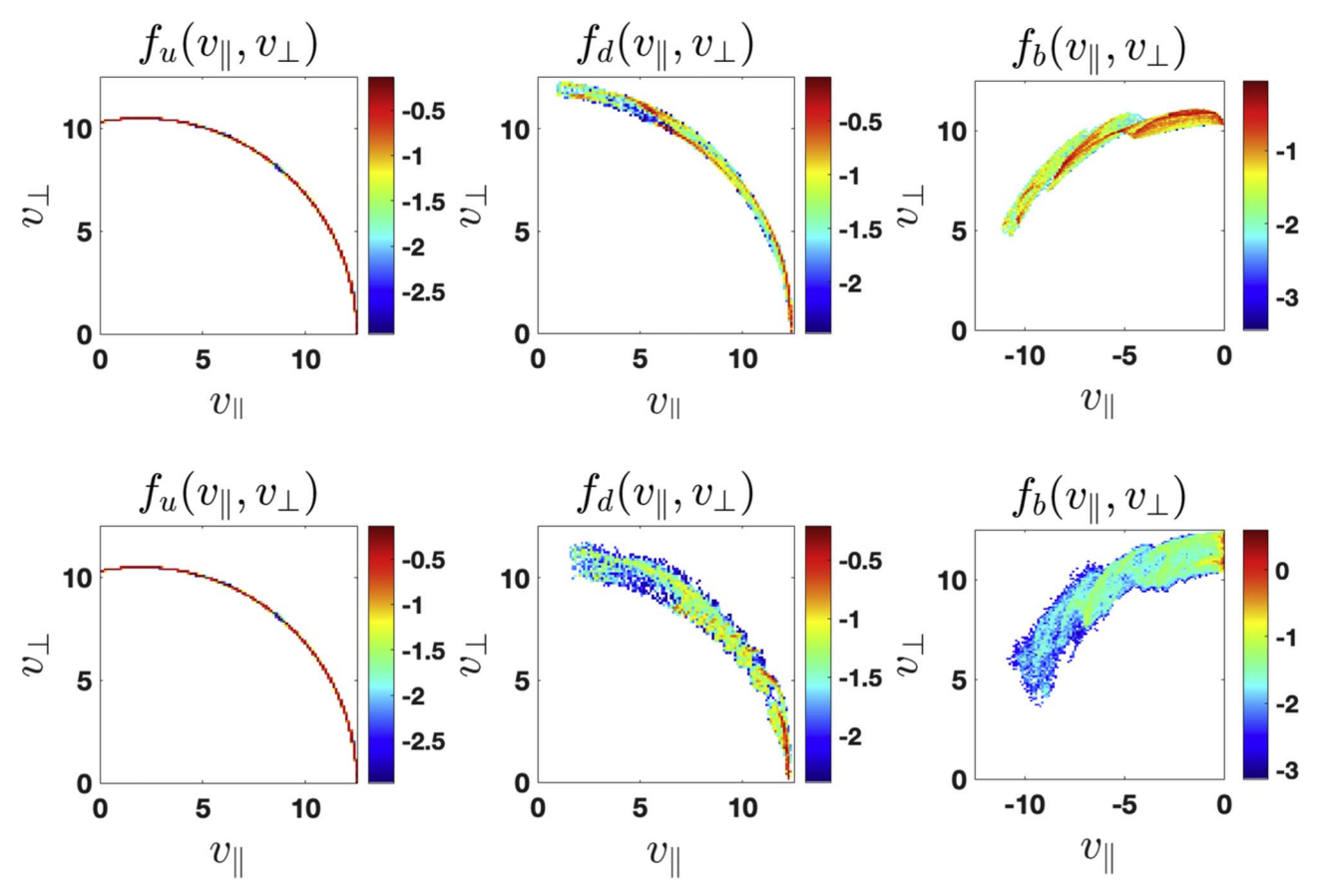


**Figure 5.** Left column: the distribution of the forward-moving incident ions  $f_u(v_{\parallel}, v_{\perp})$  (see explanation in text). Upper middle: the distribution of the ions far downstream of the shock  $f_d(v_{\parallel}, v_{\perp})$  without rippling. Bottom middle: the distribution of the ions far downstream of the shock  $f_d(v_{\parallel}, v_{\perp})$  in the rippled shock. Upper right: the distribution of the backstreaming ions  $f_b(v_{\parallel}, v_{\perp})$  without rippling. Bottom right: the distribution of the backstreaming ions  $f_b(v_{\parallel}, v_{\perp})$  in the rippled shock. The initial ion distribution is isotropic with  $v_p = 10.5$ .

# 6. Conclusions

Rippling may enhance the production of backstreaming ions in high-Mach-number shocks, even for large obliquity, and thus is a viable mechanism for ion injection into further diffusive shock acceleration. The presence of superthermal tails in the upstream ion distribution would also significantly increase the efficiency of the mechanism. This enhancement is substantial for low-energy incident ions and is expected to depend on the rippling parameters. On the other hand, for highenergy ions, which already participate in DSA, the effect of rippling is weak and not sensitive to the rippling parameters, while the reflection and formed distributions are determined by the overall change in the magnitude and direction of the magnetic field between the two asymptotic upstream and downstream regions. These findings, together with the earlier studied models of nonstationary shocks (Gedalin et al. 2016), indicate that the dynamics of high-energy ions are not sensitive to the structure of the shock transition.

Investigation of the dependence of the influence of rippling on low-energy superthermal ions on the rippling parameters is beyond the scope of the present paper and will be done in a separate study.

### Acknowledgments

M.G. was partially supported by NSF-BSF grant 2019744. M.G. and N.G. were partially supported by the European Union's Horizon 2020 research and innovation program under

grant agreement No. 101004131 (SHARP) and by the International Space Science Institute (ISSI) in Bern, through ISSI International Team project #23-575. N.P. was supported, in part, by NSF-BSF award 2010450 and NASA grant 80NSSC18K1649. N.P. was additionally supported by the IBEX mission as a part of NASA's Explorer program. V.R. was partially supported by NASA grant 80NSSC18K1649 and NSF-BSF award 2010144.

#### ORCID iDs

Michael Gedalin https://orcid.org/0000-0003-1236-4787 Natalia Ganushkina https://orcid.org/0000-0002-9259-850X Nikolai V. Pogorelov https://orcid.org/0000-0002-

6409-2392 September 10 https://orgid.org/0000-0002

Vadim Roytershteyn https://orcid.org/0000-0003-1745-7587

## References

Burgess, D. 1987, AnGeo, 5, 133

Drury, L. O. 1983, RPPh, 46, 973

Gedalin, M., Dröge, W., & Kartavykh, Y. Y. 2016, ApJ, 825, 149

Gedalin, M., & Ganushkina, N. 2022a, JPIPh, 88, 905880501

Gedalin, M., & Ganushkina, N. 2022b, JPlPh, 88, 905880301

Gedalin, M., Liverts, M., & Balikhin, M. A. 2008, JGR, 113, 05101

Gedalin, M., Pogorelov, N. V., & Roytershteyn, V. 2021, ApJ, 910, 107

Gedalin, M., Pogorelov, N. V., & Roytershteyn, V. 2023, ApJ, 951, 65

```
Gieseler, U. D. J., Kirk, J. G., Gallant, Y. A., & Achterberg, A. 1999, A&A, 345, 298

Gingell, I., Schwartz, S. J., Burgess, D., et al. 2017, JGR, 77, 736

Hudson, P. D. 1965, MNRAS, 131, 23

Johlander, A., Schwartz, S. J., Vaivads, A., et al. 2016, PhRvL, 117, 165101

Johlander, A., Vaivads, A., Khotyaintsev, Y. V., et al. 2018, PPCF, 60, 125006

Kirk, J., & Dendy, R. 2001, JPhG, 27, 1589

Kucharek, H., Möbius, E., Scholer, M., et al. 2004, AnGeo, 22, 2301

Leroy, M. M., & Winske, D. 1983, AnGeo, 1, 527

Lobzin, V. V., Krasnoselskikh, V. V., Musatenko, K., & Dudok de Wit, T. 2008, AnGeo, 26, 2899

Malkov, M., & Völk, H. 1998, AdSpR, 21, 551

Meziane, K., Wilbur, M., Mazelle, C., et al. 2004, JGR, 109, A05107

Moullard, O., Burgess, D., Horbury, T. S., & Lucek, E. A. 2006, JGR, 111,
```

```
Nicolaou, G., Livadiotis, G., Owen, C. J., Verscharen, D., & Wicks, R. T. 2018, ApJ, 864, 3
Ofman, L., & Gedalin, M. 2013, JGR, 118, 5999
Omidi, N., Desai, M., Russell, C. T., & Howes, G. G. 2021, JGR, 126, e2021JA029287
Scholer, M., Kucharek, H., & Trattner, K. J. 1998, AdSpR, 21, 533
Tanaka, M., Goodrich, C. C., Winske, D., & Papadopoulos, K. 1983, JGR, 88, 3046
Thomsen, M. F., Gosling, J. T., Bame, S. J., et al. 1983, GeoRL, 10, 1207
Treumann, R. A. 2009, A&ARv, 17, 409
Wilson, L. B. I., Stevens, M. L., Kasper, J. C., et al. 2018, ApJS, 236, 41
Zhou, X., Gedalin, M., Russell, C. T., Angelopoulos, V., & Drozdov, A. Y.
```

2020, JGR, 125, e28174